Energy Level Structure of Er^{3+} Free Ion and Er^{3+} Ion in Er_2O_3 Crystal

G. Gaigalas, D. Kato, P. Jönsson, P. Rynkun, L. Radžiūte

(Received - May 15, 2014)

NIFS-DATA-115 June 20, 2014

Energy level structure of Er^{3+} free ion and Er^{3+} ion in Er_2O_3 crystal

G. Gaigalas[a,b], D. Kato[a], P. Jönsson[c], P. Rynkun[b], L. Radžiūtė[b]

[a] *National Institute for Fusion Science, 322-6 Oroshi-cho, Toki 509-5292, Japan*
[b] *Vilnius University, Institute of Theoretical Physics and Astronomy, A. Goštauto 12, LT-01108 Vilnius, Lithuania*
[c] *Materials Science and Applied Mathematics, Malmö University, 20506 Malmö, Sweden*

Abstract

The latest version of the GRASP2K atomic structure package [P. Jönsson, G. Gaigalas, J. Bieroń, C. Froese Fischer, I.P. Grant, Comput. Phys. Commun. 184 (2013) 2197], based on the multiconfigurational Dirac-Hartree-Fock method, is extended to account for effects of crystal fields in complex systems. Energies from relativistic configuration interaction calculations are reported for the Er^{3+} free ion. E2 and M1 line strengths, weighted oscillator strengths, and rates are presented for transitions between states of the $[Xe]4f^{11}$ configuration. Also Stark levels of the Er^{3+} $^4I^o_{15/2}$ state in Er_2O_3 are calculated in the *ab initio* point charge crystal field approximation. In all calculations the Breit interaction and leading QED effects are included as perturbations. Different strategies for describing electron correlation effects are tested and evaluated. The final results are compared with experiment and other methods.

Keywords: Er^{3+}, Er_2O_3, energy structure, transition rates, crystal field effects, relativistic configuration interaction, multiconfiguration Dirac-Hartree-Fock

Preprint submitted to Atomic Data and Nuclear Data Tables

Contents

1. Introduction

The rare earth ions in ionic crystals show very sharp lines in absorption as well as emission spectra. In many cases, the line widths are as narrow as lines emitted by free ions. This feature is very different from rather broad spectra of defects in solids, such as F-centers. As suggested in [1], it means that in principle it is possible to investigate interactions between the ions and crystal fields by optical methods with a degree of accuracy similar to that possible with free atoms and ions. Trivalent erbium Er^{3+}, studied in this paper, is also one of such the rare earth ions whose spectra of free ions [2] and those of ions in a variety of host compounds [3] have been measured.

Since it was found that hydrogen permeation is reduced drastically by an oxide Er_2O_3 layer (1 μm) on metallic substrates [4], the erbium oxide is a primary candidate of tritium permeation barriers of blanket systems in nuclear fusion devices. To evaluate degradation or durability as the permeation barrier, it is essential to characterize crystallinity change inside the oxides due to neutron irradiation anticipated in the nuclear fusion devices. Recently, degradation of the crystallinity by high energy ion bombardment was inferred from ion beam induced luminescence spectra [5, 6]. To characterize the crystallinity change inside the target oxide, we need to know luminescence spectra in the damaged crystals, which is, however, hitherto unknown. Motivation of this work is to develop a theoretical method to predict ion spectra in the damaged crystals. To this end, we need to use ab-inito methods for calculations of free ion spectra in order to investigate crystal field effects without recourse to empirical parameters in atomic energy terms. Then, Stark level splitting of the atomic energy terms is investigated using the point-charge crystal field approach for a perfect crystal of the erbium oxide whose crystallographic data is available from databases [7].

Most authors [8–15] have used semi-empirical methods to obtain spectroscopic data for the free ion Er^{3+}. These methods rely on measurements of Stark components in different types of erbium doped crystals (LaF_3, $LaCl_3$, $LiYF_3$ and $ZnGa_2O_4$) that determine centers of gravity. Then, by using different approximations, the energy spectrum is derived for the free ion. The situation is similar for the Stark components themselves. The components are measured in experiments and to obtain higher levels, the Wybourne theory [16] and Superposition Models (SPM) [17] are used.

The modern highly developed experimental accuracy of determining a number of spectroscopic constants of atoms and ions requires the theoretical results to be correspondingly accurate. That accuracy can be achieved by accounting jointly for relativistic and correlation effects. There is a whole series of theoretical methods considering correlation effects in many-electron atoms and ions: different versions of the many-body perturbation theory, the configuration interaction method, the random phase approximation with exchange, the incomplete variable separation method, multiconfiguration approximation, etc. Recently the majority of theoretical *ab initio* calculations of energy spectra of atoms and ions with open shells have been carried out using configuration interaction (CI), multiconfiguration Hartree-Fock [18, 19] (MCHF) or multiconfiguration Dirac-Hartree-Fock [20, 21] (MCDHF) methods. As a rule, relativistic effects are taken into account by the MCDHF method. Usually in carrying out the calculations the well-known program GRASP2K [22] (A General-Purpose Relativistic Atomic Structure program) is used. Our analysis demonstrates that the configuration interaction method and the GRASP2K [22] package are the best tools for the investigation of the crystal field effects in ionic solids. These methods are based on the accurate four-component one-electron radial wave functions which were calculated including correlation and relativistic effects. In order to realize the project aims we modified the GRASP2K package and added a new crystal field program.

The basic, and novel, idea of this work is to calculate the energy spectrum and the transition parameters for the

free ion Er^{3+} in an *ab initio* approach and then apply the point charge crystal field as a perturbation to obtain the Er_2O_3 Stark components of the $[Xe]4f^{11}\ {}^4I^o_{15/2}$ level. The calculations are based on the MCDHF method and relativistic configuration interaction. Principles of this method for spectrum and transition calculations are presented in sections 2 and 3, respectively. Methodologies and strategies how include electron correlation effect are presented in section 4. This is followed by an evaluation of data and comparison with results of other authors in section 5. Finally, the E2 and M1 transition line strengths, weighted oscillator strengths, and rates for transitions between states of the configuration $[Xe]4f^{11}$ are presented in section 6. The point charge crystal field approach is presented in section 7 and the program based on this approximation is presented in section 8. Results for the Stark components of the $4f^{11}\ {}^4I^o_{15/2}$ level are presented and compared with the semi-empirical results of other authors in section 9. All results summarized in the conclusions section 10.

2. Computational procedure

The multiconfiguration Dirac-Hartree-Fock (MCDHF) method has recently been reviewed by Grant [20], and here we just give a brief outline. Starting from the Dirac-Coulomb Hamiltonian

$$H_{\rm DC} = \sum_{i=1}^{N} \left(c\,\boldsymbol{\alpha}_i \cdot \boldsymbol{p}_i + (\beta_i - 1)c^2 + V_i^N \right) + \sum_{i>j}^{N} \frac{1}{r_{ij}}, \tag{1}$$

where V^N is the monopole part of the electron-nucleus Coulomb interaction, the atomic state functions (ASFs), describing different fine-structure states, are obtained as linear combinations of symmetry adapted configuration state functions (CSFs)

$$|\gamma J M_J\rangle = \sum_{k=1}^{N_{CSFs}} c_k |\gamma_k J M_J\rangle. \tag{2}$$

In the expression above J and M_J are the angular quantum numbers and γ denotes other appropriate labeling of the configuration state function, for example parity, orbital occupancy, and coupling scheme. The configuration state functions are built from products of one-electron Dirac orbitals. In the relativistic self-consistent field (RSCF) procedure both the radial parts of the Dirac orbitals and the expansion coefficients are optimized to self-consistency. The Breit interaction

$$H_{\rm Breit} = -\sum_{i<j}^{N} \left[\boldsymbol{\alpha}_i \cdot \boldsymbol{\alpha}_j \frac{\cos(\omega_{ij} r_{ij}/c)}{r_{ij}} \ + (\boldsymbol{\alpha}_i \cdot \boldsymbol{\nabla}_i)(\boldsymbol{\alpha}_j \cdot \boldsymbol{\nabla}_j) \frac{\cos(\omega_{ij} r_{ij}/c) - 1}{\omega_{ij}^2 r_{ij}/c^2} \right] \tag{3}$$

as well as leading QED corrections, vacuum polarization and self-energy, can be included in subsequent relativistic configuration interaction (RCI) calculations [23]. Calculations can be done for single states, but also for portions of a spectrum in the extended optimal level (EOL) scheme, where optimization is on a weighted sum of energies [24]. Using the latter scheme a balanced description of a number of fine-structure states belonging to one or more configurations can be obtained in a single calculation.

In relativistic calculations the states are given in jj coupling (ASF). To adhere to the labeling conventions used by the experimentalists, the ASFs are transformed from the jj coupling to the LS coupling using the methods developed in [25, 26]. All calculations were performed with the GRASP2K code [22].

3. Computation of transition parameters

The transition parameters, such as rates for spontaneous decay, for multipole transitions between two atomic states $\gamma J M_J$ and $\gamma' J' M'_J$ can be expressed in terms of reduced transition matrix elements

$$\left[\gamma J \| \mathbf{Q}_k^{(\lambda)} \| \gamma' J'\right], \tag{4}$$

where $\mathbf{Q}_k^{(\lambda)}$ is the electromagnetic multipole operator of rank k in length or velocity gauge [27]. The superscript designates the type of multipole: $\lambda = 1$ for electric multipoles and $\lambda = 0$ for magnetic multipoles. Standard Racah algebra assumes that the atomic state functions are built from the same orthogonal radial orbital set [28]. However, this restriction can be relaxed. To compute transition matrix elements between two atomic state functions described by independently optimized orbital sets, transformations of the atomic state functions are performed in such a way that the orbital sets become biorthogonal, in which case the calculation can be handled using standard techniques [29].

4. Calculations

In this work calculations were done by configuration, i.e. wave functions for all states belonging to a specific configuration were determined simultaneously in an EOL calculation [24]. The configuration expansions were obtained using the active set method [13, 30]. Here CSFs of a specified parity and J symmetry are generated by substitutions of orbitals in a number of reference configurations with orbitals in an active set. By applying restrictions on the allowed substitutions, different electron correlation effects can be targeted. To monitor the convergence of the calculated energies and transition parameters, the active sets were increased in a systematic way by adding layers of correlation orbitals.

A careful analysis showed that the states of the Er^{3+} ion were well described in a single reference configuration Dirac-Hartree-Fock (DHF) model. In the section below different strategies for generating the configuration expansions from the reference configuration are described. In all calculations the orbitals of the reference configuration were taken from the initial DHF calculation. The energy functional, on which the orbitals were optimized, was the weighted energy average of two lowest states with J=1/2, the six lowest states with J=3/2, the seven lowest states with, respectively, J=5/2, 7/2, 9/2, the five lowest states with J=11/2, the three lowest states with J=13/2, three lowest with J=15/2, and finally the lowest state with J=17/2.

1. **S V strategy** – the CSFs were generated by single (S) substitutions from the valence shell ($4f$ shell) to active sets with principal quantum numbers $n = 5, 6, 7, 8, 9$ and angular symmetries p, f, h, k (the orbitals s, d, g, i leads to the configurations with opposite symmetry in the case of single substitutions). In this strategy the inactive core is $1s^2 2s^2 2p^6 3s^2 3p^6\ 3d^{10} 4s^2 4p^6 4d^{10} 5s^2 5p^6$. The RSCF calculations for each layer of orbitals were followed by RCI calculations, including the Breit interaction and QED corrections. At all steps only new orbitals were optimized. The results of these calculations are presented in Table A.
2. **SD VV strategy** – the CSFs were generated by single and double (SD) substitutions from the valence shell ($4f$ shell) to active sets with principal quantum numbers $n = 5, 6, 7$ and angular symmetries s, p, d, f. In this strategy the inactive core is again $1s^2 2s^2 2p^6 3s^2 3p^6\ 3d^{10} 4s^2 4p^6 4d^{10} 5s^2 5p^6$. The RSCF calculations for each layer of orbitals were followed by RCI calculations, including the Breit interaction and QED corrections. At all steps only new orbitals were optimized. The results of these calculations are presented in Table A.

3. **S V+C strategy** – the CSFs were generated by S substitutions from the core shells ($5s$, $5p$ shells) and the valence shell ($4f$ shell) to active sets with principal quantum numbers $n = 5, 6, 7, 8, 9$ and angular symmetries s, p, d, f, g, h, i. In this strategy the inactive core is $1s^2 2s^2 2p^6 3s^2 3p^6 3d^{10} 4s^2 4p^6 4d^{10}$. The RSCF calculations for each layer of orbitals were followed by RCI calculations, including the Breit interaction and QED corrections. At all steps only new orbitals were optimized. The results of these calculations are presented in Table B.
4. **SD VV+CC+CV strategy** – the CSFs were generated by SD substitutions from the core shells ($5s$, $5p$ shells) and the valence shell ($4f$ shell) to active sets with principal quantum numbers $n = 5, 6$ and angular symmetries s, p, d, f, g, h. In this strategy the inactive core is $1s^2 2s^2 2p^6 3s^2 3p^6 3d^{10} 4s^2 4p^6 4d^{10}$. The radial orbitals were taken from the S V+C strategy and RCI calculations, including the Breit interaction and QED corrections, were done. The results of these calculations are presented in Table B.
5. **SD V+C+CV strategy** – the CSFs were generated by SD substitutions from the core shells ($5s$, $5p$ or other closed core shells that were opened step by step as presented in the tables) and the valence shell ($4f$ shell) to active sets with principal quantum numbers $n = 5, 6$ and angular symmetries s, p, d, f, g, h. Double (D) substitutions were restricted in such a way, that one excitation would be from the core and another from the valence shell. The radial orbitals were taken from the S V+C strategy and RCI calculations, including the Breit interaction and QED corrections, were done. The results of these calculations are presented in Tables C–D.

5. Results and evaluation of data

The results from the calculations using the S V and SD VV strategies, the S V+C and SD VV+CC+CV strategies, and, finally, the SD V+C+CV strategies are shown, respectively, in Table A, Table B, and Tables C–D. The tables display the convergence of the energies with respect to the increasing n quantum number of the active sets of orbitals. In the last column of the tables the energies from NIST [31] are given. At the bottom of the tables the expansion size N_{CSF} (number of CSFs) is displayed for each calculation.

The ion subject to the analysis in this paper has previously not been thoroughly investigated. To the knowledge of the authors there have been practically no publications on *ab initio* theoretical calculations or experimental results for isolated Er^{3+}. The experimental energy levels for this ion are instead taken as experimental centers of gravity for several erbium doped crystals. Therefore the reliability of the present MCDHF and RCI calculations can not be systematically evaluated with the help of other independent sources. Taking this into account, results based on the different strategies, including calculations with various types of correlations and substitutions to large active sets, need to be internally compared and benchmarked.

As can be seen from the tables the results obtained from different strategies differ considerably from the values in the NIST database [31]. The results obtained in the single substitution valence (the case S V) and single, double substitutions valence-valence (the case SD VV) approximations agree poorly with experiment. The results are converged at $n = 6$, and a further extension of the active set does not change the results. Adding valence-valence (the case SD VV) correlation to the valence correlation leads to an insignificant (approx. 0.5%) change of the energy levels. However, if core correlation is included (the case S V+C), the positions of the energy levels approach the experimental values (approx. 5%). The exceptions are levels 2 and 3, where even valence and valence-valence correlations (the case S V and SD VV) give precise predictions. Influence of core-core and core-valence correlations (the case SD VV+CC+CV) for the

Table A

Energy levels for Er^{3+} from RCI calculations including S V and SD VV correlation: LSJ denote leading LS term and J value of the level. All listed energies (in cm^{-1}) of the levels are relative to the ground level.

LSJ	DHF	**S V**					**SD VV**			NIST
		$n=5$	$n=6$	$n=7$	$n=8$	$n=9$	$n=5$	$n=6$	$n=7$	[31]
$^4I_{15/2}$	0	0	0	0	0	0	0	0	0	0
$^4I_{13/2}$	6207	6204	6217	6225	6225	6225	6255	6272	6279	6480
$^4I_{11/2}$	10155	10168	10162	10172	10171	10171	10168	10176	10181	10110
$^4I_{9/2}$	12965	12998	12956	12967	12964	12964	12928	12921	12922	12350
$^4F_{9/2}$	19084	18693	17940	17944	17937	17937	18451	18132	18082	15180
$^4S_{3/2}$	23696	23279	22776	22781	22777	22777	22996	22658	22610	18290
$^2H_{11/2}$	22402	22484	22113	22121	22109	22109	21975	21804	21764	
$^4F_{7/2}$	25030	24459	23571	23579	23575	23579	24347	23970	23918	20400
$^4F_{5/2}$	27091	26512	25596	25605	25602	25602	26376	25986	25932	22070
$^4F_{3/2}$	27351	26950	26127	26137	26130	26130	26741	26369	26316	22410
N_{CSF}	41	1229	4443	7657	12200	16743	21153	120888	302868	

Table B

Energy levels for Er^{3+} from RCI calculations including S V+C and SD VV+CC+CV correlation: $4d$ means, that the $4d$ shell is open for single and double substitutions. LSJ denote leading LS term and J value of the level. All listed energies (in cm^{-1}) of the levels are relative to the ground level.

LSJ	**S V+C**					**SD VV+CC+CV**			NIST
	$n=5$	$n=6$	$n=7$	$n=8$	$n=9$	$n=5$	$n=6$	$4d$ $n=5$	[31]
$^4I_{15/2}$	0	0	0	0	0	0	0	0	0
$^4I_{13/2}$	6215	6214	6220	6221	6221	6379	6391	6502	6480
$^4I_{11/2}$	10133	10131	10140	10143	10142	10268	10233	10332	10110
$^4I_{9/2}$	12913	12891	12902	12904	12904	12957	12827	12889	12350
$^4F_{9/2}$	17809	16993	17001	17001	17001	17335	16490	16764	15180
$^4S_{3/2}$	21904	21340	21350	21351	21351	21459	20623	20650	18290
$^2H_{11/2}$	21845	21484	21503	21504	21504	21305	20716	20747	
$^4F_{7/2}$	23421	22403	22414	22416	22415	23074	22048	22511	20400
$^4F_{5/2}$	25383	24345	24359	24361	24361	25013	23937	24406	22070
$^4F_{3/2}$	25780	24866	24879	24880	24880	25364	24355	24695	22410
N_{CSF}	5853	18438	32120	45802	59484	634453	4311822	2230820	

Table C

Energy levels for Er^{3+} from RCI calculations including SD V+C+CV correlations: 5^* means, that all shells from the core with $n = 5$ are open for single and double substitutions. LSJ denote leading LS term and J value of the level. All listed energies (in cm^{-1}) of the levels are relative to the ground level.

LSJ	5^*			5^*4d				5^*4d4p		
	$n=5$	$n=6$	$n=7$	$n=5$	$n=6$	$n=7$	$n=8$	$n=5$	$n=6$	$n=7$
$^4I_{15/2}$	0	0	0	0	0	0	0	0	0	0
$^4I_{13/2}$	6195	6200	6207	6305	6258	6278	6260	6322	6291	6312
$^4I_{11/2}$	10102	10106	10116	10165	10163	10192	10183	10118	10153	10187
$^4I_{9/2}$	12876	12860	12871	12844	12891	12922	12931	12738	12838	12877
$^4F_{9/2}$	17773	16953	16959	17100	16684	16687	16771	16796	16490	16502
$^4S_{3/2}$	21915	21338	21346	21018	20992	21000	21125	20007	20226	20250
$^2H_{11/2}$	21778	21411	21429	21148	21193	21218	21306	20696	20856	20899
$^4F_{7/2}$	23368	22350	22361	22730	22072	22084	22156	22426	21900	21919
$^4F_{5/2}$	25322	24284	24297	24642	23988	24005	24086	24244	23744	23770
$^4F_{3/2}$	25732	24815	24827	24984	24514	24531	24623	24444	24167	24196
N_{CSF}	10882	32155	56275	40517	106047	187856	269665	66407	174558	308987

Table D

Energy levels for Er^{3+} from RCI calculations including SD V+C+CV correlation: 4^* or/and 3^* means, that all shells from the core with $n = 4$ or/and $n = 3$ are open for single and double substitutions. LSJ denote leading LS term and J value of the level All listed energies (in cm^{-1}) of the levels are relative to the ground level.

LSJ	4^*			4^*3d		4^*3d3p		4^*3^*		4^*3^*2p	$4^*3^*2^*$	NIST
	$n=5$	$n=6$	$n=7$	$n=5$	$n=6$	$n=5$	$n=6$	$n=5$	$n=6$	$n=5$	$n=5$	[31]
$^4I_{15/2}$	0	0	0	0	0	0	0	0	0	0	0	0
$^4I_{13/2}$	6323	6291	6313	6326	6301	6329	6312	6328	6311	6328	6328	6480
$^4I_{11/2}$	10110	10144	10179	10106	10156	10105	10166	10104	10165	10104	10104	10110
$^4I_{9/2}$	12724	12825	12866	12707	12835	12704	12842	12703	12841	12703	12703	12350
$^4F_{9/2}$	16768	16457	16473	16698	16446	16679	16427	16678	16425	16678	16678	15180
$^4S_{3/2}$	19960	20158	20187	19856	20139	19809	20093	19807	20089	19807	19807	18290
$^2H_{11/2}$	20632	20779	20827	20575	20774	20553	20753	20549	20748	20549	20549	
$^4F_{7/2}$	22398	21860	21884	22320	21855	22301	21838	22300	21835	22300	22300	20400
$^4F_{5/2}$	24200	23680	23710	24116	23673	24091	23652	24089	23647	24089	24089	22070
$^4F_{3/2}$	24401	24110	24145	24311	24102	24282	24078	24280	24074	24280	24280	22410
N_{CSF}	77272	202141	357885	134340	354974	181369	474742	198197	519450	252756	273079	

higher levels is at the 2% level, however the position of the first three levels coincide with experiment (see Fig. 1 and Tables A-D).

Attention should also be drawn to the positions of $^4S_{3/2}$ and $^2H_{11/2}$ in various approximations. It is obvious that in the cases S V and SD VV, independent of the size of the active set, the positions of these levels do not agree with experiment (see Table A). However, after adding core correlation with an active set $n = 6$, the positions become correct (see Table B). Adding valence, core and core-valence effects, when at least the level $4d$ is opened, leads to correct positions for theses levels already at $n = 5$. (see Tables B and D).

The change of the positions of levels 5 and 6 when increasing the active sets and opening deeper closed shells is demonstrated in Fig. 2 and Tables A-D. It is seen that calculations with the active set $n = 6$ including single and double substitutions from the valence, core and core-valence shells, when only $4d$ and $4p$ excitations are taken from the core (the case SD V+C+CV $4d$ $4p$), lead to energy level positions close to the experimental ones. In addition, in this approximation, the order of the levels $^4S_{3/2}$ and $^2H_{11/2}$ agree with the results of the experiment (see Table E). Further increase of the active set or opening of deeper core shells do not significantly change the results (see Fig. 2). As a matter of fact, similar results for the above mentioned levels are obtained in the SD VV+CC+CV approximation when $n = 6$ (single and double substitutions from the valence, valence-valence, core, core-core and core-valence shells in the active set $n = 6$). But in the above mentioned case, the ASFs consist of 4 311 822 CSF whereas in the case of SD V+C+CV $4d$ $4p$ only of 174 558. Hence, core-core, and valence-valence correlations are less important than valence, core and core-valence.

Table E compares computed energy levels with results from other theories and experiment. Levels are notated in the form $^{(2S+1)}L_J^{Nr}$ where, instead of the group labels νWU, single character "numbers" Nr are used [32]. In Table E the levels we identify with $^2G^1_{9/2}$ and $^4G^1_{9/2}$ were by authors [8–12, 14] originally identified with $^2H_{9/2}$, and $^2G_{9/2}$ respectively. In a similar way the level we identify as $^2H^2_{9/2}$ was originally identified with $^4G_{9/2}$ in papers [9–11]. The level identifications in Table E are based on an LS composition analysis, that will be further discussed in the next section. Experimental data [8] for centers of gravity (Exp. gravity centers) were obtain by measuring Stark levels of the Er^{3+} absorption spectrum in LaF_3 at 77 K. Only those lines which persist at 4.2 K were retained. The Stark levels of $^4I_{13/2}$ were obtained in another way. In this case the center was determined from fluorescence lines. Most transitions in the spectrum are from the $^4I_{15/2}$ ground state Stark components to the excited levels Stark components. In the paper [9] the authors have extended the measured absorption spectrum in the same crystal into the ultraviolet region up to 2000 Å. Thus, more excited levels were obtained. Similar experiments were done on other systems. The absorption and fluorescence spectra of $ErCl_3$ diluted by $LaCl_3$ were measured by [10, 11] and from the absorption spectrum of Er^{3+} doped in $LiYF_3$ [12] the centers of gravity were determined.

Experimental data of free ion Er^{3+} were obtained by [1] from Arc spectra. In this case the column is labeled Ex. With the help of small variations of parameters (F_2, F_4, F_6 and ζ), originally described by Wybourne [33], the free ion spectrum [8, 9] was determined from the experimental centers of gravity data described above ([8, 9]). The eigenstates and the corresponding energy levels [15] were found (in LSJ coupling) by diagonalizing the interaction matrix describing the spin-orbit and electrostatic energies. The spin-orbit parameter ζ and the Racah parameters E^1, E^2, E^3 were determined in a fitting procedure in which centers of gravity were taken from [8] and [9]. Semi-empirical data for the spectrum in [14] were evaluated by measuring the Er^{3+} center of gravity in $ZnGa_2O_4$. Semi-empirical data in the table are marked SE.

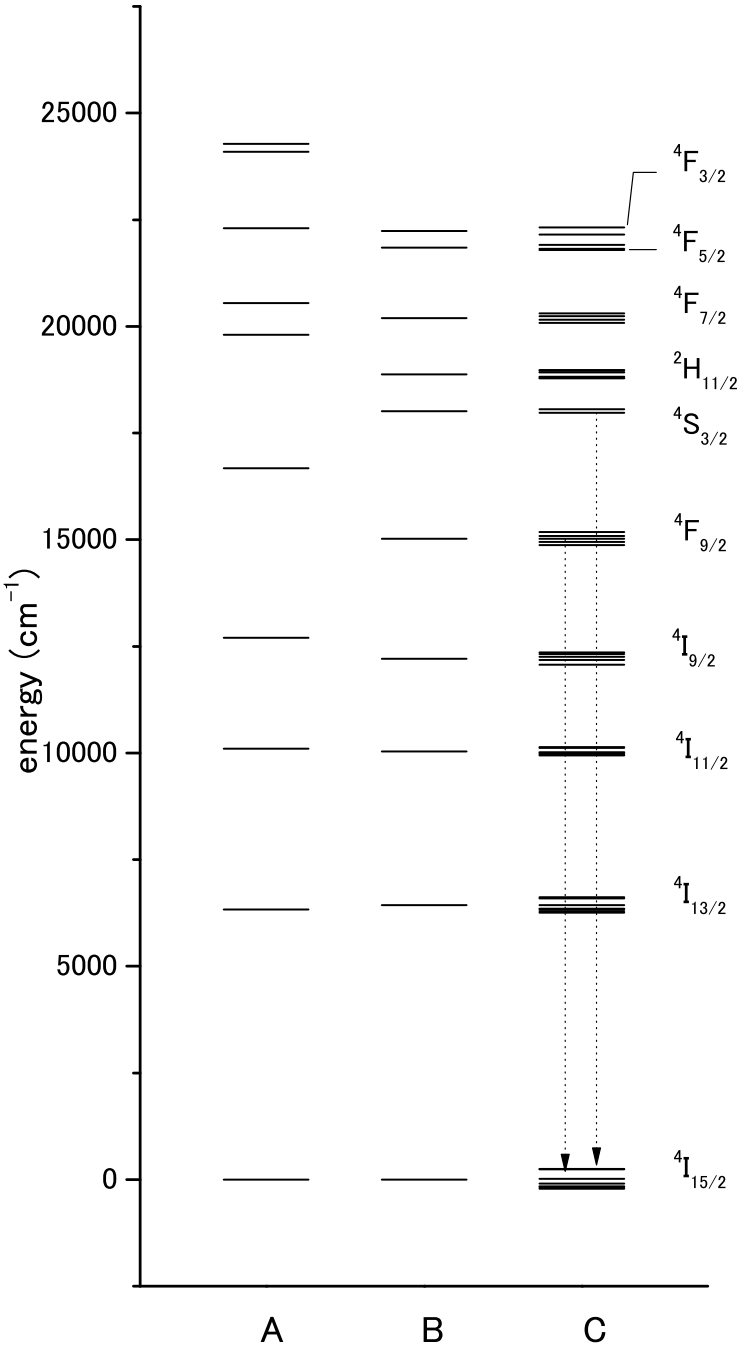

Fig. 1: Energy levels of Er^{3+}. A - energy spectra of Er^{3+}. B - averaged energies from crystal field calculations. C - energy spectra of Er^{3+} in crystal field.

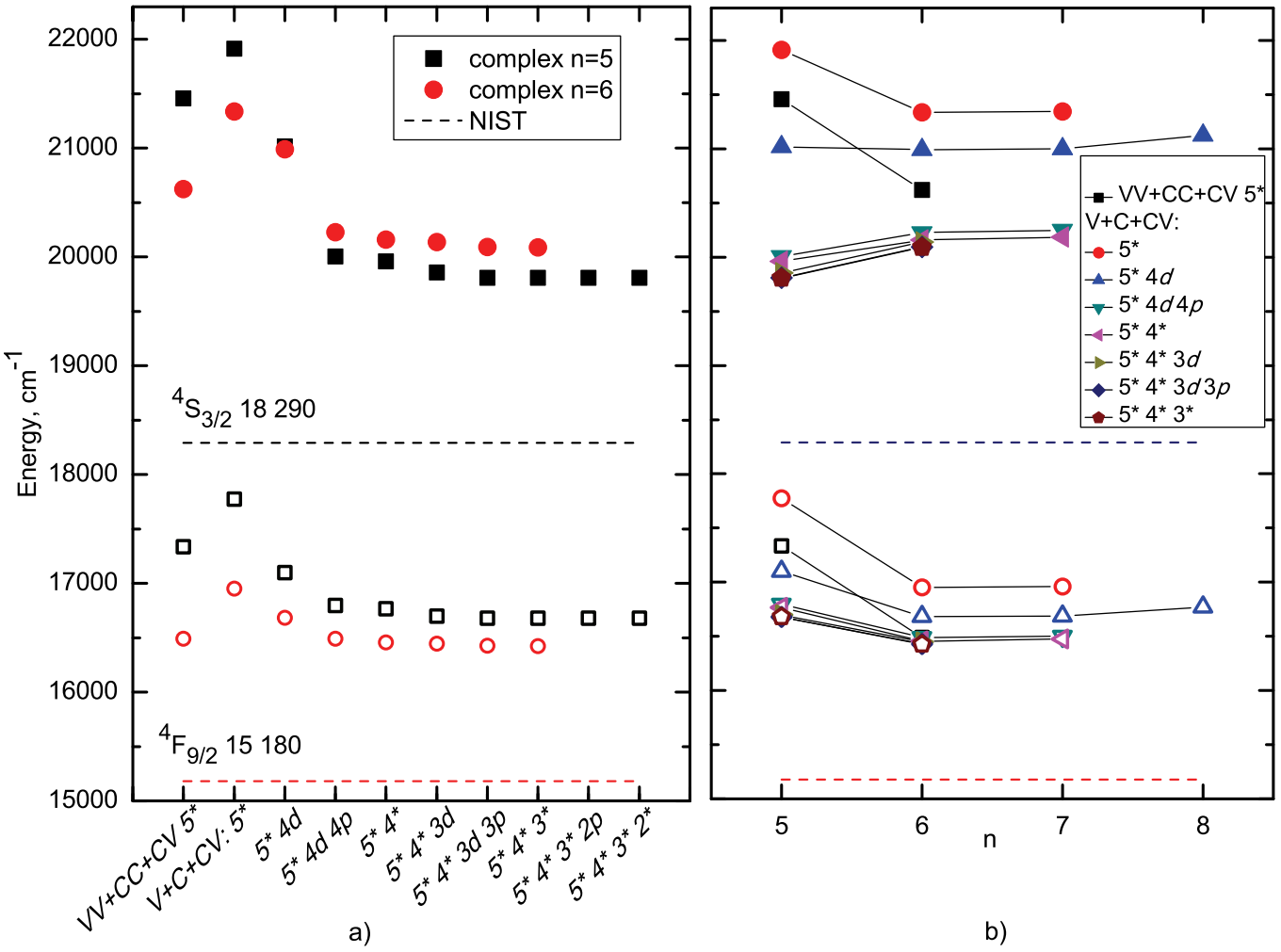

Fig. 2: Convergence of the energy for $4f^{11}\ {}^4S_{3/2}$ (filled symbols) and ${}^4F_{9/2}$ (empty symbols) levels of Er^{3+}: a) opening core shells and b) increasing principal quantum number of the active set in different strategies. In one case, notated $VV + CC + CV$, SD excitation were made without restrictions. In the other cases double substitutions were restricted in such a way, that one excitation would be from the core and another from the valence shell.

The MCDHF and RCI calculations (Th.) of the positions of the first three levels agree with experiment. For the higher levels the agreement is less satisfactory. But while comparing theory and experiment it is necessary to consider the fact that the free ions calculations are done exclusively in this paper. The remaining results are obtained when the Er^{3+} ion exists in different crystal materials. Experimental energy levels for Er^{3+} are given as experimental centers of gravity for LaF_3, $LaCl_3$ and $LiYF_3$. Energy levels given at NIST [31] are derived from the spectrum of Er^{3+} in LaF_3 [35].

Table F gives compositions of the ASFs in jj- and LS- coupling. In the table also the quantum "number" Nr is used. Numbers in parenthesis show shell J values in jj-coupling. For example J values of $4f^3_-$ shell can be 3/2 (see the string $4f^3_-(3/2)4f^8$ in to the line 27), 5/2 (see the string $4f^3_-(5/2)4f^8$ in to the line 18), and 9/2 (see the string $4f^3_-(9/2)4f^8$ in to the line 4). Mixing coefficients are given in percentage.

For a given set of ASFs with the same J and parity, the CSFs with the largest expansion coefficient is selected. The quantum numbers of this CSFs are used as the label for the corresponding ASF. The corresponding CSF is removed from consideration and the procedure is repeated until all ASFs are labeled. The label for the last ASF may be based on a CSF contribution that is exceedingly small. For example levels in jj-coupling: $^4F^1_{5/2}$, $^2G^1_{9/2}$, $^2G^1_{7/2}$, $^2D^1_{5/2}$ and $^2D^1_{3/2}$; in LS-coupling: $^2G^1_{7/2}$ and $^2H^2_{9/2}$.

Levels are identified with an accuracy of at least 99%, but shown in Table F are only those CSFs with coefficients greater than or equal to 10%. An exception is the $^4F^1_{5/2}$ level. Here we see CSFs with a 3% contribution because levels with larger coefficients were already assigned. The evaluation of the suitability of the couplings for the classification of energy spectra is performed using the method described in [34]. The square of the largest coefficient is averaged over the states (P_s) of the configurations considered, and a mean-square deviation (R) of the intermediate coupling scheme from the pure one serve as the numerical parameters describing the suitability of the coupling scheme. In this study we used the parameter

$$P_s = \frac{\sum{}'(2J+1)P_J}{\sum{}'(2J+1)}, \tag{5}$$

where

$$P_J = \frac{1}{m_J}\sum_{i=1}^{m_J} c^2_{ind\ i}. \tag{6}$$

Here m_J stands for the number of ASFs with certain J and $c_{ind\ i}$ is the expansion coefficient of the CSF that was used to label level i (see eq. 6). In most case $c_{ind\ i}$ is the largest coefficient, but in some case: jj-coupling: $^4F^1_{5/2}$, $^2G^1_{9/2}$, $^2G^1_{7/2}$, $^2D^1_{5/2}$ and $^2D^1_{3/2}$; in LS-coupling: $^2G^1_{7/2}$ and $^2H^2_{9/2}$, it is not. The values of the parameter P_s for LS is 0.82 and for jj-coupling 0.67. The parameters show, for levels of the Er^{3+} configuration $[Xe]4f^{11}$, that LS-coupling is more preferable than jj-coupling. But in some cases, even using LS-coupling, identification is a bit complicated.

6. Transition parameters

The states of the $[Xe]4f^{11}$ configuration undergo M1 and E2 transitions. The line strengths S, weighted oscillator strengths gf, and transition rates A_{ki} in s^{-1}, computed based on wave functions from the S V + C strategy with $n = 9$ and from the SD VV + CC + CV strategy with $n = 5$, are displayed in Tables G - I. The transition rates are all very weak, of the order 10^1 s^{-1} for the M1 transitions, and a magnitude smaller for E2. As can be seen from Tables H and I

Table E

Comparison of centers of gravity with energy levels obtained by semi-empirical methods and our levels computed in the *ab initio* approach including SD V+C+CV correlations. The error bars estimated by comparing the data with NIST.

LSJ	Exp. gravity centers				Exp.	SE				Th.	NIST	Err.
	[8]	[9]	[10, 11]	[12]	[1]	[8]	[9]	[15]	[14]	4*3* $n=6$	[31]	(in %)
$^4I^1_{15/2}$	0	0	0	0	0	0	0	0	0	0	0	
$^4I^1_{13/2}$	6484	6481	6482	6495	6485	6540	6502	6405	6511	6311	6480	2.6
$^4I^1_{11/2}$	10111	10123	10111	10140	10123	10123	10125	10022	10043	10165	10110	0.5
$^4I^1_{9/2}$	12356	12351	12351	12380	12345	12328	12340	12241	12003	12841	12350	4.0
$^4F^1_{9/2}$	15241	15236	15174	15260	15182	15266	15181	15076	14913	16425	15180	8.2
$^4S^1_{3/2}$	18360	18353	18291	18355	18299	18433	18427	18320	18018	20089	18290	9.8
$^2H^2_{11/2}$	19124	19118	19036	19120	19010	19166	19284	19175	18851	20748		
$^4F^1_{7/2}$	20506	20492	20407	20505	20494	20524	20327	20123	20034	21835	20400	7.0
$^4F^1_{5/2}$	22170	22162	22066	22155	22181	22065	21990	21870	21713	23647	22070	7.1
$^4F^1_{3/2}$	22502	22494	22408		22453	22477	22344	22227	21978	24074	22410	7.4
$^2G^1_{9/2}$	24535	24527	24457	24550	24475	24539	24537	24322	23874	25987		
$^4G^1_{11/2}$		26369	26263		26376	26615	26447	26327	25929	28291		
$^4G^1_{9/2}$		27412	27219		27319	27663	27431	27305		29369		
$^2K^1_{15/2}$			27498		27584	27041	27293	27176		29713		
$^2G^1_{7/2}$		28082	27879		27825		27994	27877		30255		
$^2P^1_{3/2}$		31501	31389		31414		31605	31477		33797		
$^2K^1_{13/2}$			32856				32521	32392		34993		
$^4G^1_{5/2}$		32922					33315	33178		35584		
$^2P^1_{1/2}$								33336		35829		
$^4G^1_{7/2}$		33995	33836		33849	28110	33918	33783		35959		
$^2D^1_{5/2}$		34838	34648				34794	34641		37550		
$^2H^2_{9/2}$		36424	36332				36408	36268		37974		
$^4D^1_{5/2}$		38610					38649	38526		42247		
$^4D^1_{7/2}$		39314					39205	39067		43125		
$^2I^1_{11/2}$							40309	40164		44363		
$^2L^1_{17/2}$							40664	40508		44686		
$^2D^1_{3/2}$							42199	42802		44985		
$^4D^1_{3/2}$							42946	42044		46361		
$^2I^1_{13/2}$							42947	42797		46509		
$^4D^1_{1/2}$								46808		50552		
$^2L^1_{15/2}$							46836	46667		50695		
$^2H^1_{9/2}$								46989		51680		
$^2D^2_{5/2}$								48873		52987		
$^2H^1_{11/2}$								50061		54438		
$^2D^2_{3/2}$								54910		58851		
$^2F^2_{7/2}$								55055		60100		
$^2F^2_{5/2}$								62909		68234		
$^2G^2_{7/2}$								64688		72071		
$^2G^2_{9/2}$								68765		75942		
$^2F^1_{5/2}$								93134		103064		
$^2F^1_{7/2}$								96726		107321		

Table F

The ASFs compositions of 41 lowest levels of Er^{3+} in *jj*- and *LS*- coupling.

Level	*Composition in jj-coupling*	*Composition in LS-coupling*
$^4I^1_{15/2}$	**74** $4f^6_-4f^5(15/2)$+**23** $4f^5_-4f^6(6)$	**96**
$^4I^1_{13/2}$	**75** $4f^5_-4f^6(6)$+ **15** $4f^5_-4f^6(4)$	**98**
$^4I^1_{11/2}$	**42** $4f^4_-(4)4f^7$+**23** $4f^5_-4f^6(6)$+**18** $4f^6_-4f^5(11/2)$	**87**+**10** $^2H^2$
$^4I^1_{9/2}$	**29** $4f^4_-(4)4f^7$ + **28** $4f^6_-4f^5(9/2)$+**15** $4f^5_-4f^6(2)$+**13** $4f^3_-(9/2)4f^8$+**12** $4f^5_-4f^6(4)$	**71**+**15** $^2H^2$
$^4F^1_{9/2}$	**55** $4f^6_-4f^5(9/2)$+**22** $4f^5_-4f^6(4)$+**12** $4f^5_-4f^6(6)$	**69**+**12** $^4I^1$+**11** $^2G^1$
$^4S^1_{3/2}$	**53** $4f^6_-4f^5(3/2)$+**31** $4f^5_-4f^6(4)$+**12** $4f^4_-(2)4f^7$	**74**+**15** $^2P^1$
$^2H^2_{11/2}$	**57** $4f^6_-4f^5(11/2)$+**24** $4f^4_-(4)4f^7$+**12** $4f^5_-4f^6(4)$	**53**+**31** $^4G^1$+**10** $^4I^1$
$^4F^1_{7/2}$	**62** $4f^5_-4f^6(4)$+**16** $4f^5_-4f^6(6)$+**10** $4f^4_-(2)4f^7$	**92**
$^4F^1_{5/2}$	**3** $4f^5_-4f^6(2)$+**44** $4f^5_-4f^6(4)$+**21** $4f^4_-(2)4f^7$+**19** $4f^6_-4f^5(5/2)$+ **9** $4f^4_-(4)4f^7$	**86**+**10** $^2D^1$
$^4F^1_{3/2}$	**36** $4f^5_-4f^6(4)$+**30** $4f^5_-4f^6(2)$+**14** $4f^6_-4f^5(3/2)$+**12** $4f^4_-(4)4f^7$	**68**+**18** $^2D^1$+**12** $^4S^1$
$^2G^1_{9/2}$	**13** $4f^5_-4f^6(4)$+**31** $4f^5_-4f^6(6)$+**18** $4f^4_-(4)4f^7$+**13** $4f^3_-(9/2)4f^8$+**11** $4f^6_-4f^5(9/2)$	**18**+**23** $^2H^2$+**21** $^4F^1$+**15** $^2G^2$+**11** $^4I^1$
$^4G^1_{11/2}$	**62** $4f^5_-4f^6(6)$+**17** $4f^4_-(2)4f^7$+**10** $4f^4_-(4)4f^7$	**64**+**23** $^2H^2$
$^4G^1_{9/2}$	**42** $4f^5_-4f^6(6)$+**23** $4f^5_-4f^6(4)$+**15** $4f^5_-4f^6(2)$	**80**+**12** $^2H^2$
$^2K^1_{15/2}$	**60** $4f^5_-4f^6(6)$+**24** $4f^6_-4f^5(15/2)$+**15** $4f^4_-(4)4f^7$	**91**
$^2G^1_{7/2}$	**22** $4f^6_-4f^5(7/2)$+**26** $4f^4_-(2)4f^7$+**19** $4f^5_-4f^6(2)$+**15** $4f^5_-4f^6(4)$	**27**+**40** $^4G^1$+**24** $^2G^2$
$^2P^1_{3/2}$	**36** $4f^4_-(2)4f^7$+**29** $4f^6_-4f^5(3/2)$ + **21** $4f^4_-(4)4f^7$	**39**+**24** $^2D^1$+**20** $^4F^1$+**10** $^4S^1$
$^2K^1_{13/2}$	**52** $4f^5_-4f^6(4)$+**45** $4f^4_-(4)4f^7$	**91**
$^4G^1_{5/2}$	**30.39** $4f^4_-(4)4f^7$+**23** $4f^5_-4f^6(2)$+**21** $4f^5_-4f^6(0)$+**16** $4f^3_-(5/2)4f^8$	**92**
$^2P^1_{1/2}$	**90** $4f^5_-4f^6(2)$	**91**
$^4G^1_{7/2}$	**92** $4f^4_-(4)4f^7$	**55**+**26** $^2G^1$+**15** $^2G^2$
$^2D^1_{5/2}$	**26** $4f^6_-4f^5(5/2)$+**29.80** $4f^4_-(4)4f^7$+**20** $4f^4_-(2)4f^7$+**18** $4f^5_-4f^6(2)$	**69**+**11** $^4F^1$+**10** $^2D^2$
$^2H^2_{9/2}$	**60** $4f^3_-(9/2)4f^8$+**28** $4f^4_-(4)4f^7$	**31**+**24** $^2G^1$+**16** $^2G^2$+**14** $^4G^1$
$^4D^1_{5/2}$	**50** $4f^5_-4f^6(4)$+ **33** $4f^6_-4f^5(5/2)$	**50**+**28** $^2D^2$+**18** $^2D^1$
$^4D^1_{7/2}$	**53** $4f^5_-4f^6(6)$ +**26** $4f^6_-4f^5(7/2)$	**94**
$^2I^1_{11/2}$	**71** $4f^5_-4f^6(4)$+**14** $4f^6_-4f^5(11/2)$	**68**+**27** $^2H^1$
$^2L^1_{17/2}$	**98** $4f^5_-4f^6(6)$	**98**
$^2D^1_{3/2}$	**25** $4f^4_-(4)4f^7$+**34** $4f^3_-(3/2)4f^8$+**25** $4f^4_-(2)4f^7$+**10** $4f^5_-4f^6(2)$	**45**+**30** $^2P^1$+**15** $^4D^1$
$^4D^1_{3/2}$	**50** $4f^5_-4f^6(2)$+**19** $4f^5_-4f^6(4)$+**12** $4f^4_-(2)4f^7$+**11** $4f^4_-(4)4f^7$	**60**+**25** $^2D^2$+**12** $^2P^1$
$^2I^1_{13/2}$	**44** $4f^4_-(4)4f^7$+**31** $4f^5_-4f^6(4)$+**23** $4f^5_-4f^6(6)$	**91**
$^4D^1_{1/2}$	**89** $4f^4_-(4)4f^7$	**91**
$^2L^1_{15/2}$	**82** $4f^4_-(4)4f^7$+**15** $4f^5_-4f^6(6)$	**93**
$^2H^1_{9/2}$	**47** $4f^5_-4f^6(2)$+**25** $4f^4_-(2)4f^7$+**19** $4f^5_-4f^6(4)$	**78**+**17** $^2H^2$
$^2D^2_{5/2}$	**45** $4f^4_-(2)4f^7$+**23** $4f^4_-(4)4f^7$+**11** $4f^5_-4f^6(2)$	**48**+**37** $^4D^1$
$^2H^1_{11/2}$	**69** $4f^4_-(2)4f^7$+**20** $4f^4_-(4)4f^7$	**58**+**29** $^2I^1$+**10** $^2H^2$
$^2D^2_{3/2}$	**51** $4f^3_-(3/2)4f^8$+ **27** $4f^4_-(4)4f^7$+ **13** $4f^4_-(2)4f^7$	**70**+**20** $^4D^1$
$^2F^2_{7/2}$	**40** $4f^4_-(2)4f^7$+**24** $4f^6_-4f^5(7/2)$ +**14** $4f^5_-4f^6(6)$ +**12** $4f^4_-(0)4f^7$	**55**+**35** $^2F^1$
$^2F^2_{5/2}$	**66** $4f^3_-(5/2)4f^8$+**25** $4f^5_-4f^6(2)$	**62**+**20** $^2F^1$+**11** $^2D^2$
$^2G^2_{7/2}$	**60** $4f^5_-4f^6(2)$ + **12** $4f^5_-4f^6(4)$+**11** $4f^6_-4f^5(7/2)$	**56**+**39** $^2G^1$
$^2G^2_{9/2}$	**50** $4f^4_-(2)4f^7$+**17** $4f^5_-4f^6(2)$+**11** $4f^5_-4f^6(6)$+**10** $4f^5_-4f^6(4)$	**55**+**40** $^2G^1$
$^2F^1_{5/2}$	**64** $4f^5_-4f^6(0)$+ **17** $4f^5_-4f^6(2)$+**11** $4f^3_-(5/2)4f^8$	**72**+**25** $^2F^2$
$^2F^1_{7/2}$	**58** $4f^4_-(0)4f^7$+**18** $4f^4_-(2)4f^7$+**10** $4f^6_-4f^5(7/2)$	**58**+**37** $^2F^2$

Table G

Transition data in Er^{3+} for E2 transitions (S V+C strategy $n = 9$): Leading LS term and J for lower level i, upper level k, wavelength λ (in Å), line strength S (length form), weighted oscillator strength gf (length form), transition rate A_{ki} (length form) in s^{-1}, δT accuracy indicator.

Levels		J		λ	S	gf	A_{ki}	δT
i	k	i	k	(Å)			(s^{-1})	
$^2H^o$	$^2F^o$	9/2	5/2	1857.66	4.678×10^{-1}	1.225×10^{-8}	3.947	0.22323
$^2H^o$	$^2F^o$	11/2	7/2	1803.91	3.983×10^{-1}	1.139×10^{-8}	2.919	0.14592
$^4G^o$	$^2F^o$	7/2	5/2	1310.09	4.899×10^{-2}	3.658×10^{-9}	2.370	0.62902
$^2H^o$	$^2F^o$	9/2	7/2	1175.28	2.981×10^{-2}	3.083×10^{-9}	1.861	0.65372
$^4G^o$	$^2F^o$	7/2	5/2	1413.64	4.886×10^{-2}	2.904×10^{-9}	1.615	0.61265
$^4F^o$	$^2F^o$	9/2	7/2	1057.54	1.498×10^{-2}	2.127×10^{-9}	1.586	0.59905
$^2H^o$	$^2F^o$	9/2	7/2	1368.18	5.205×10^{-2}	3.412×10^{-9}	1.520	0.64047
$^2H^o$	$^2F^o$	11/2	7/2	1110.41	1.770×10^{-2}	2.170×10^{-9}	1.467	0.40245
$^2P^o$	$^2F^o$	1/2	5/2	1442.12	4.729×10^{-2}	2.647×10^{-9}	1.415	0.86168
$^2I^o$	$^2F^o$	11/2	7/2	1525.92	7.895×10^{-2}	3.731×10^{-9}	1.336	0.39214

the transition parameters for the M1 transition are comparatively stable to correlation effects. The parameters for the E2 transition are given in the length gauge. As an indication of the accuracy the quantity

$$\delta T = \frac{|S_l - S_v|}{\max(S_l, S_v)} \tag{7}$$

is displayed. Here S_l and S_v are the line strengths in, respectively, the length and the velocity gauges. It has been argued that δT is an initial and rough estimate of the uncertainties of the computed line strengths, which in this case would translate to uncertainties up to 40 %. No theoretical or experimental transition parameters are available for the Er^{3+} free ion. The fact that strong spectral lines are observed for Er^{3+} doped in crystals indicates that the crystal field has a very large influence on the transition strengths.

7. Method of accounting for the crystal field effects

In order to calculate the splitting of the ionic energy levels γJ in solids, the crystal field effects must be included. Instead of using the simplified treatment of the crystal field effects based on the Stevens' operator-equivalent method [36, 37] we used the fully *ab-initio* method. Treating the external ions as point charges at fixed positions, the crystal field operator can be presented in the following form in a. u. [38]:

$$H_{CF} = -\sum_{j=1}^{A}\sum_{i=1}^{N} \frac{Z_j}{\left|\vec{R}_j - \vec{r}_i\right|}$$

Table H

Transition data in Er^{3+} for M1 transitions (S V+C strategy $n = 9$): Leading LS term and J for lower level i, upper level k, wavelength λ (in Å), line strength S, weighted oscillator strength gf, transition rate A_{ki} in s^{-1}.

Levels		J		λ	S	gf	A_{ki}
i	k	i	k	(Å)			(s^{-1})
$^4G^o$	$^2F^o$	9/2	7/2	3092.11	3.182×10^{-1}	4.161×10^{-7}	3.629×10^{1}
$^4D^o$	$^2F^o$	7/2	7/2	1496.03	3.367×10^{-2}	9.101×10^{-8}	3.390×10^{1}
$^2F^o$	$^2F^o$	7/2	5/2	2227.84	7.490×10^{-2}	1.360×10^{-7}	3.045×10^{1}
$^4F^o$	$^2D^o$	7/2	5/2	5934.26	1.174	8.001×10^{-7}	2.526×10^{1}
$^4G^o$	$^2F^o$	7/2	5/2	2952.02	1.193×10^{-1}	1.634×10^{-7}	2.085×10^{1}
$^2G^o$	$^2F^o$	7/2	7/2	2727.26	1.161×10^{-1}	1.721×10^{-7}	1.930×10^{1}
$^4I^o$	$^2K^o$	15/2	15/2	3295.48	4.007×10^{-1}	4.918×10^{-7}	1.888×10^{1}
$^4I^o$	$^2H^o$	13/2	11/2	6543.55	2.211	1.366×10^{-6}	1.774×10^{1}
$^2D^o$	$^2F^o$	5/2	5/2	6477.10	8.945×10^{-1}	5.585×10^{-7}	1.480×10^{1}
$^4D^o$	$^2D^o$	7/2	5/2	9621.90	2.664	1.120×10^{-6}	1.344×10^{1}
$^2D^o$	$^2D^o$	5/2	3/2	4549.37	1.874×10^{-1}	1.666×10^{-7}	1.342×10^{1}
$^2H^o$	$^2H^o$	9/2	9/2	8335.67	2.844	1.380×10^{-6}	1.324×10^{1}
$^4G^o$	$^2F^o$	5/2	5/2	2935.34	7.319×10^{-2}	1.008×10^{-7}	1.301×10^{1}
$^2P^o$	$^2D^o$	3/2	3/2	8930.79	1.338	6.058×10^{-7}	1.267×10^{1}
$^2H^o$	$^2F^o$	9/2	7/2	2773.73	7.746×10^{-2}	1.129×10^{-7}	1.224×10^{1}
$^2H^o$	$^4G^o$	11/2	9/2	11517.70	6.861	2.409×10^{-6}	1.211×10^{1}
$^2K^o$	$^2L^o$	15/2	15/2	4666.75	7.233×10^{-1}	6.268×10^{-7}	1.200×10^{1}
$^2F^o$	$^2F^o$	5/2	7/2	2438.34	5.059×10^{-2}	8.391×10^{-8}	1.177×10^{1}
$^4S^o$	$^2P^o$	3/2	1/2	5980.98	1.827×10^{-1}	1.235×10^{-7}	1.151×10^{1}
$^4I^o$	$^2H^o$	11/2	9/2	6123.27	8.512×10^{-1}	5.621×10^{-7}	1.000×10^{1}

Table I

Transition data in Er^{3+} for M1 transitions (SD VV+CC+CV strategy $n = 5$): Leading LS term and J for lower level i, upper level k, wavelength λ (in Å), line strength S, weighted oscillator strength gf, transition rate A_{ki} in s^{-1}.

Levels		J		λ	S	gf	A_{ki}
i	k	i	k	(Å)			(s^{-1})
$^4G^o$	$^2F^o$	9/2	7/2	3226.93	3.797×10^{-1}	4.759×10^{-7}	3.810×10^{1}
$^4D^o$	$^2F^o$	7/2	7/2	1519.74	3.301×10^{-2}	8.785×10^{-8}	3.171×10^{1}
$^4F^o$	$^2D^o$	7/2	5/2	6167.16	1.388	9.101×10^{-7}	2.660×10^{1}
$^2F^o$	$^2F^o$	7/2	5/2	2217.26	6.391×10^{-2}	1.166×10^{-7}	2.636×10^{1}
$^4G^o$	$^2F^o$	7/2	5/2	2993.02	1.396×10^{-1}	1.886×10^{-7}	2.340×10^{1}
$^4I^o$	$^2H^o$	13/2	11/2	6699.57	2.773	1.674×10^{-6}	2.073×10^{1}
$^4I^o$	$^2K^o$	15/2	15/2	3306.17	4.242×10^{-1}	5.188×10^{-7}	1.978×10^{1}
$^2G^o$	$^2F^o$	7/2	7/2	2824.16	1.251×10^{-1}	1.791×10^{-7}	1.872×10^{1}
$^2D^o$	$^2D^o$	5/2	3/2	4372.58	1.938×10^{-1}	1.793×10^{-7}	1.563×10^{1}
$^2P^o$	$^2D^o$	3/2	3/2	8856.88	1.569	7.161×10^{-7}	1.522×10^{1}
$^2D^o$	$^2F^o$	5/2	5/2	6723.86	1.015	6.106×10^{-7}	1.502×10^{1}
$^2H^o$	$^4G^o$	11/2	9/2	10366.98	5.910	2.305×10^{-6}	1.431×10^{1}
$^2H^o$	$^2H^o$	9/2	9/2	8215.46	2.886	1.420×10^{-6}	1.403×10^{1}
$^4D^o$	$^2D^o$	7/2	5/2	10176.36	3.091	1.228×10^{-6}	1.319×10^{1}
$^2K^o$	$^2L^o$	15/2	15/2	4458.51	6.924×10^{-1}	6.280×10^{-7}	1.317×10^{1}
$^4G^o$	$^2F^o$	5/2	5/2	3008.30	7.323×10^{-2}	9.843×10^{-8}	1.209×10^{1}
$^4S^o$	$^2P^o$	3/2	1/2	6183.57	2.104×10^{-1}	1.376×10^{-7}	1.200×10^{1}
$^2H^o$	$^2F^o$	9/2	7/2	2811.76	7.589×10^{-2}	1.091×10^{-7}	1.151×10^{1}
$^2D^o$	$^2F^o$	5/2	7/2	1786.55	1.740×10^{-2}	3.938×10^{-8}	1.029×10^{1}
$^4I^o$	$^2H^o$	11/2	9/2	6208.26	9.111×10^{-1}	5.935×10^{-7}	1.027×10^{1}

$$= \sum_{j=1}^{A}\sum_{i=1}^{N}\sum_{k=0}^{\infty}\sum_{q=-k}^{k} (-1)^{q+1} \sqrt{\frac{4\pi}{2k+1}}\ B_k\left(r_i, R_j, Z_j\right)\ C_q^k\left(\theta_i, \phi_i\right)\ Y_{-q}^k\left(\theta_j, \phi_j\right), \tag{8}$$

where

$$B_k\left(r, R, Z\right) = Z \begin{cases} r^k/R^{k+1}; & r < R, \\ R^k/r^{k+1}; & r > R. \end{cases} \tag{9}$$

and A is the number of the external ions, Z_j and R_j, θ_j, ϕ_j are the charges and the spherical coordinates of the external ions, N stands for a number of the electrons. Charges and positions of the external ions are the parameters (which depend on the compound) in the calculations. Using first order perturbation theory (diagonalization of the H_{CF} operator matrix), splitting of the degenerate atomic energy levels (and shift of $J = 0$ state energy) in the crystal electric field (Stark effect) can be calculated.

The matrix element of the crystal field operator H_{CF} has the form:

$$\begin{aligned} &\left\langle \gamma J M_J \left| H_{CF} \right| \gamma' J' M_J' \right\rangle \\ &\qquad = \sum_{j=1}^{A}\sum_{k=0}^{j_a+j_b}\sum_{q=-k}^{k}\sum_{r,s}\sum_{a,b} c_r c_s \left(-1\right)^{J-M_J} \begin{pmatrix} J & k & J' \\ -M_J & q & M_J' \end{pmatrix} \\ &\qquad \times\sqrt{2J+1}\ d_{ab}^k\left(r,s\right)\left[\kappa_a \| C^k \| \kappa_b\right]\left(-1\right)^{q+1}\ Z_j \sqrt{\frac{4\pi}{2k+1}} \\ &\qquad \times Y_{-q}^k\left(\theta_j, \phi_j\right)\ \left(\int_0^{R_j} \frac{r^k}{R_j^{k+1}}\ \left(P_a P_b\ +\ Q_a Q_b\right)\ dr \right. \\ &\qquad \left. + \int_{R_j}^{\infty} \frac{R_j^k}{r^{k+1}}\ \left(P_a P_b\ +\ Q_a Q_b\right)\ dr \right), \end{aligned} \tag{10}$$

where

$$\left[\kappa_a \| C^k \| \kappa_b\right] = \left(-1\right)^{j_a - 1/2}\ \sqrt{2j_b\ +\ 1} \begin{pmatrix} j_a & k & j_b \\ 1/2 & 0 & -1/2 \end{pmatrix} \pi\left(l_a, l_b, k\right). \tag{11}$$

Here P_a and Q_a are the large and small components of the relativistic one-electron radial wave function, $d_{ab}^k(rs)$ are the spin-angular coefficients that arise from using Racah's algebra in the decomposition of the one-electron operator matrix element [28] and $\pi\left(l_a, l_b, k\right)$ is defined:

$$\pi\left(l_a, l_b, k\right) = \begin{cases} 1; & \text{if } l_a + k + l_b \text{ even}, \\ 0; & \text{otherwise}. \end{cases} \tag{12}$$

Degenerate γJ levels split due to the crystal field into a number of sub-levels ($a\ =\ 1, .., 2J+1$):

$$\left|\gamma_a J M_J\right\rangle_a\ =\ \sum_{k=1}^{N_{CSFs}}\sum_{m=-j}^{j} c_{km}^{(a)} \left|\gamma_k J M_J = m\right\rangle. \tag{13}$$

Using this method, splitting of energy levels (E_a) and weights (c_{ia}) can be obtained. Depending on the symmetry of the crystal some of the energy levels can also be degenerate.

Crystal field interaction also mixes different atomic state functions (ASFs) - J mixing effects. In this case taking into account ASFs the wave functions of crystal field sub-levels with different J values can be expressed:

$$|\gamma J M_J\rangle_a \;=\; \sum_{k=1}^{N_{CSFs}} \sum_{j=J_{min}}^{J_{max}} \sum_{m=-j}^{j} c^{(a)}_{kjm} |\gamma_k J = j M_J = m\rangle. \tag{14}$$

In order to be able to perform such calculations the GRASP2K [22] relativistic atomic structure programs been extended. This extension include programs for the crystal field operator matrix element calculation and diagonalization of matrix of full atomic Hamiltonian (including matrix elements between different ASFs).

8. Structure of the program CF_Hamiltonian

The GRASP2K package is written in Fortran and the new crystal field program is based on the same language, because it must become inherent part of the GRASP2K package. Along with the new modules to be created (we shall describe them later), the new program uses common libraries and subroutines of the GRASP2K package. The detailed structure of these modules is represented by Fig. 3. Modules STARTTIME, CHKPLT, SETDBG, GETMIXBLOCK, GETMIXA, GETMIXC, SETMC, FACTT, SETCON, SETSUM, SETCSLA and STOPTIME are the original modules of the program GRASP2K and perform the same functions as in the GRASP2K package. For example, after calling SETMC - to set up machine- and precision-dependent parameters and perform other-dependent initialization, SETCON - to set up physical constants and conversion factors, and FACTT - to generate a table of factorials for later use by CLRX and DRACAH. All these modules of the GRASP2K program have a auxiliary character and they organize the calculations in the crystal field approximation.

The subroutine Ions_input is reading all information about the crystal geometry from the file Crystaldata before the program calls to the main module . The calculations themselves must be performed by the module CF_Hamil (see Fig. 3).

The subroutine Y_k from Fig. 3 performs the calculation of the spherical functions Y^k_q. The routine MATEL_CF_Hamil computes the spin-angular part of reduced matrix elements of the crystal field operator. It calls to the utility CLRX for getting the value of the coefficient

$$C(a,k,b) = \begin{pmatrix} j_a & k & j_b \\ \frac{1}{2} & 0 & -\frac{1}{2} \end{pmatrix}. \tag{15}$$

The sub-programme IONS_Param collects the specific crystal-dependent values of the A (the number of the external ions), Z_j (the charge of the external ions) and R_j, θ_j, ϕ_j (the coordinates of the external ions). Namely this subroutine contains the information on the parameters of concrete crystal. If there is a need to consider crystals of the same symmetry, one has to change the values of the parameters mentioned above. Thus, such algorithm allows easily to extend the domain of tasks to be considered. The calculation of the linear combination of radial integrals

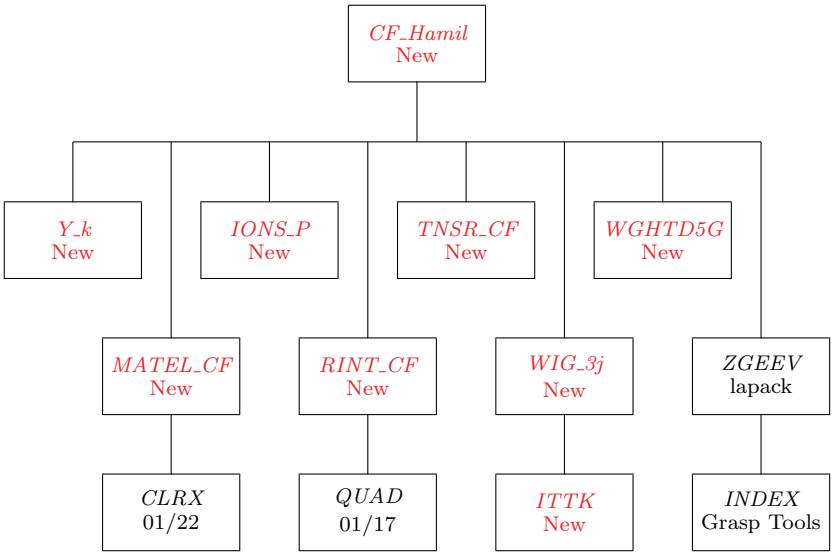

Fig. 3: Structure of subroutine CF_HAMIL: the new modules of program are marked in read.

$$\int_0^{R_j} \frac{r^k}{R_j^{k+1}} \left(P_a P_b + Q_a Q_b\right) dr + \int_{R_j}^{\infty} \frac{R_j^k}{r^{k+1}} \left(P_a P_b + Q_a Q_b\right) dr \tag{16}$$

of crystal field operator is carried out by the routine RINT_CF_HAMIL. The standard subroutine QUAD is the utility routine that performs finite-difference quadratures $\int_0^\infty f(r)dr$ for given $f(r)$.

Module TNSR_CF contains two subroutines (ONESCALAR and ONEPARTICLEJJ_CF) which perform the spin-angular integration of one-particle operator. The subroutine ONESCALAR is located in the RANG library from the GRASP2K package and the subroutine ONEPARTICLEJJ_CF is the modification of subroutine ONEPARTICLEJJ from the RANG. The routine WIG_3J calculates the Wigner 3-j symbol. The routine ITTA checks triangular conditions $I + J \geq K$, $I + K \geq J$ and $J + K \geq I$.

Subroutine ZGEEV is from the library LAPACK. It compute the eigenvalues and the left and/or right eigenvectors of a general complex matrix generalized eigenproblem.

9. Calculations of the crystal-field splitting of Er^{3+} ion in the Er_2O_3 compound

In this paper, Stark component splitting of the $4f^{11}\ {}^4I_{15/2}$ level for Er^{3+} in Er_2O_3 crystal field in the point charge crystal field approximation is analyzed. The crystal field parameters were taken from AMCSD [7]. In all Tables of Stark components, wave functions and corresponding energy level are designated by the label of the M_J with the largest expansion coefficients $c_{km}^{(a)}$ or $c_{kjm}^{(a)}$ (see eq. 13 or 14). Labels determined in this manner may not be unique.

For the calculations done in this paper, various computational schemes, which to certain extent included correlation effects, were used (see Tables J-M). The simplest approximation used in this paper was the Dirac-Hartree-Fock method. While gradually increasing correlations, Stark splitting increases. The results are most significantly affected by the core

Table J

Energy (Stark) levels (in cm^{-1}) of Er^{3+} ($4f^{11}\ {}^4I^o_{15/2}$) in Er_2O_3 crystal field (6 without J mix).

J	M_J	DHF	**S V**	**S V+C**	**SD V+C+CV**	
			$n=5$	$n=5$	$n=5$	$n=6$
15/2	±1/2	0.00	0.00	0.00	0.00	0.00
15/2	±7/2	286.23	341.52	463.29	460.68	492.90
15/2	±11/2	485.07	578.63	804.59	799.90	856.37
15/2	±15/2	629.63	750.41	1061.75	1055.36	1130.66
15/2	±15/2	753.49	898.71	1269.39	1261.88	1350.97
15/2	±11/2	955.70	1141.85	1579.00	1570.31	1677.84
15/2	±7/2	1256.59	1503.96	2015.92	2005.70	2138.97
15/2	±1/2	1475.21	1765.32	2383.69	2371.41	2529.70

and the valence correlations. Their total influence (S V+C) in some cases reach up to 60%. The core-valence (CV) correlations are not very important.

The calculations included different number of neighbor atoms. In one case the point charge crystal field was made with the help of 6 neighbor atoms (see Table J and K) and in another case with the help of 740 879 neighbor atoms (see Table L and M). More neighbor atoms leads to bigger splitting (approx. 7%).

For the ASF the J quantum number is not a good quantum number because the operator of the point charge crystal field does not commute with the angular momentum operator J. Thus, in this paper calculations were done with a mixing of all J values $(1/2 - 17/2)$ of the configuration $4f^{11}$ (see eq. 14). Results of calculations with mixed J values are displayed in Tables K and M. The results without mixing are given in Tables J and L. Mixing of J increases the Stark effect splitting up to 6%. It is revealed that influence of the configuration state functions with opposite parity (P) to the Stark splitting is very small. The effect of the parity mixing on the transition rates is not considered here, but will be in focus in future work.

Table N compares the results obtained in this study with the results of other authors using semi-empirical methods as well as with the experimental results. Experimental data of Stark components were obtained for single crystals Er_2O_3 and Er^3:Y_2O_3 [39]. Semi-empirical Stark levels were calculated using a Hamiltonian containing atomic and crystal field terms. The crystal field Hamiltonian is defined in Wybourne notation [16]. In other experiments, Er_2O_3 powder was used [40]. Experiments have shown that the powders also exhibited the cubic symmetry of the Er_2O_3 crystal. Data from experiment were used in semi-empirical methods to compute crystal field parameters and Stark levels. In another experiment the Stark components of lowest tree levels were measured by absorption spectroscopy in Er_2O_3 and ErF_3 [41], more components were obtained by SPM [17].

As can be seen from the comparative analysis of the results, the *ab-initio* point charge crystal field approximation for Er^{3+} in Er_2O_3 leads to a bigger splitting compared with the experimental one (see Fig. 1). In order to get more accurate theoretical results, the further development of the theory is needed.

Table K

Energy (Stark) levels (in cm^{-1}) of Er^{3+} ($4f^{11}\ {}^4I^o_{15/2}$) in Er_2O_3 crystal field (6 with J mix).

J	M_J	DHF	**S V**	**S V+C**	**SD V+C+CV**	
			$n=5$	$n=5$	$n=5$	$n=6$
15/2	±1/2	0.00	0.00	0.00	0.00	0.00
15/2	±7/2	278.13	329.30	440.33	437.81	464.70
15/2	±11/2	457.13	537.55	726.05	721.45	758.51
15/2	±15/2	571.20	667.71	910.25	904.19	947.90
15/2	±15/2	708.34	837.14	1153.41	1146.45	1214.37
15/2	±11/2	930.76	1107.42	1515.03	1506.60	1603.02
15/2	±7/2	1232.84	1470.66	1958.54	1948.41	2071.22
15/2	±1/2	1438.49	1713.00	2298.27	2286.00	2427.59

Table L

Energy (Stark) levels (in cm^{-1}) of Er^{3+} ($4f^{11}\ {}^4I^o_{15/2}$) in Er_2O_3 crystal field (740879 without J mix).

J	M_J	DHF	**S V+C**	**SD V+C+CV**			
			$n=5$	$n=5$	4*3*2* $n=5$	$n=6$	$n=7$
15/2	±1/2	0.00	0.00	0.00	0.00	0.00	0.00
15/2	±7/2	309.12	495.96	493.29	490.72	527.41	528.48
15/2	±11/2	517.69	854.13	849.31	845.51	908.74	908.82
15/2	±15/2	670.00	1123.40	1116.81	1111.97	1195.82	1195.25
15/2	±15/2	802.19	1344.47	1336.69	1330.81	1430.37	1428.60
15/2	±11/2	1018.35	1677.48	1668.37	1660.49	1782.22	1779.09
15/2	±7/2	1334.44	2142.31	2131.47	2120.57	2273.31	2269.96
15/2	±1/2	1575.32	2547.48	2534.35	2521.31	2703.65	2698.40

Table M

Energy (Stark) levels (in cm^{-1}) of Er^{3+} ($4f^{11}\ {}^4I^o_{15/2}$) in Er_2O_3 crystal field (740879 with J mix).

J	M_J	DHF	**S V+C**	**SD V+C+CV**			
			$n=5$	$n=5$	4*3*2* $n=5$	$n=6$	$n=7$
15/2	±1/2	0.00	0.00	0.00	0.00	0.00	0.00
15/2	±7/2	299.78	469.00	466.42	462.71	494.01	495.38
15/2	±11/2	486.38	764.09	759.38	749.59	795.88	797.41
15/2	±15/2	606.55	957.04	950.86	937.69	995.29	995.97
15/2	±13/2	754.60	1223.86	1216.64	1206.22	1288.70	1287.26
15/2	±11/2	994.67	1617.43	1608.58	1599.14	1712.46	1709.93
15/2	±7/2	1313.71	2093.92	2083.12	2070.17	2216.61	2213.95
15/2	±1/2	1542.22	2472.25	2459.08	2441.85	2613.83	2609.69

Table N

Comparison of computed energy (Stark) levels (in cm^{-1}) of Er^{3+} ($4f^{11}\ {}^4I^o_{15/2}$) in Er_2O_3 crystal field with other theories and experiment.

Experiment			Semi-empirical			Theoretical
[39]	[40]	[41]	[39]	[40]	[41]	**SD V+C+CV** $n=7$
0	0	0	1	2	0	0.00
38	36	39.5	36	37	11.6	495.38
75	69	75.3	66	65	79.4	797.41
88	86	89.0	93	81	107.7	995.97
159	162	260.1	169	157	154.8	1287.26
265	263	349.6	262	265	176.7	1709.93
490	484	488.6	477	483	194.3	2213.95
505	503	531.2	502	506	249.8	2609.69

10. Conclusions

MCDHF method was used to compute energy spectrum and to calculate line strengths, weighted oscillator strengths, and transitions rates for E2 and M1 transitions between states of the $[Xe]4f^{11}$ configuration of the Er^{3+} free ion. Influences of different types of correlation effects are presented in Tables A - D and Figure 2. Analysis of these data show, that values of free ion Er^{3+} energy levels converge, when core is opened up to 5* 4* 3* and important correlations such as S V+C+CV are included. Comparing with experiment and semi-empirical results we see that our *ab initio* calculations for the energy spectrum agree to within 9.8 % for the free ion. By analysis of ASFs composition of levels in Er^{3+}, we obtain that more preferable is LS-coupling, than jj-coupling.

The GRASP2K package was extended by applying the point charge crystal field approach for obtaining Er^{3+} ion in Er_2O_3 Stark component of $[Xe]4f^{11}\ ^4I^o_{15/2}$ levels. Stark splitting calculations were performed including different types of correlation effect. Labeling of Stark component was done with M_J and J (assigning M_J with biggest mixing coefficient).

In this work calculations were done with J mixing, too. This additional mixing changed the Stark splitting up to 6%. The mixing of configuration state functions with different parity is small, and does not influence the final energy values of the Stark component. Point charge crystal field approximation for Er^{3+} in Er_2O_3 in our calculations give bigger splitting of the Stark component than the experimental one, so the further development of the theory is needed.

References

[1] S. Hüfner, Optical Spectra of Transparent Rare-earth Compounds, Academic, New York, 1978.

[2] H.M. Crosswhite and H.W. Moos, Conf. Opt. Properties Ions in Crystals, Wiley (Interscience), New York, 1967/

[3] S. Hüfner, Z. Phys. **168** (1962) 74.

[4] D. Levchuk et al., J. Nucl. Mater. **367** (2007) 1033.

[5] T. Tanaka et al., J. Nucl. Mater. **417** (2011) 794.

[6] D. Kato et al., Plasma and Fusion Res. **7** (2012) 2405043.

[7] R.T. Downs and M. Hall-Wallace, The American Mineralogist Crystal Structure Database, `http://rruff.geo.arizona.edu/AMS/amcsd.php` American Mineralogist **88** (2003) 247.

[8] W.F. Krupke and J.B. Gruber, J. Chem. Phys. **39** (1963) 1024.

[9] W.F. Krupke and J.B. Gruber, J. Chem. Phys. **41** (1964) 1225.

[10] F. Varsanyi and G.H. Dieke, J. Chem. Phys. **36** (1962) 2951.

[11] G.H. Dieke and S. Singh, J. Chem. Phys. **35** (1961) 555.

[12] M.R. Brown, K.G. Roots and W.A. Shand, J. Phys. C: Solid State Phys. **2** (1969) 593.

[13] J. Olsen, B.O. Roos, P. Jorgensen, and H.J.Aa Jensen, J. Chem. Phys. **89** (1988) 2185.

[14] M. Vasile, N. Avram, P. Vlazan, I. Grozescu and M. Miclau, J. of Optoelectronics and Advanced Materials **10** (2008) 2898.

[15] M.J. Weber, Phys. Rev. A **157** (1967) 262.

[16] B. G. Wybourne, Spectroscopic properties of rare earths, Wiley, New York, 1966.

[17] D. J. Newman and B. Ng, Rep. Prog. Phys. **52** (1989) 699.

[18] C. Froese Fischer, The Hartree-Fock method for atoms, Wiley, New York, 1977.

[19] C. Froese Fischer, G. Tachiev, G. Gaigalas and M.R. Godefroid, Comput. Phys. Commun. **559** (2007) 176.

[20] I.P. Grant, Relativistic Quantum Theory of Atoms and Molecules, Springer, New York, 2007.

[21] I.P. Grant, Methods in Computational Chemistry, Vol. 2, Plenum Press, New York, 1988, pp. 1-71.

[22] P. Jönsson, G. Gaigalas, J. Bieroń, C. Froese Fischer, and I.P. Grant, Comput. Phys. Commun. **184** (2013) 2197.

[23] B.J. McKenzie, I.P. Grant, and P.H. Norrington, Comput. Phys. Commun. **21** (1980) 233.

[24] K.G. Dyall, I.P. Grant, C.T. Johnson, F.A. Parpia, and E.P. Plummer, Comput. Phys. Commun. **55** (1989) 425.

[25] G. Gaigalas, T. Žalandauskas, and S. Fritzsche, Comput. Phys. Commun. **157** (2004) 239.

[26] G. Gaigalas, T. Žalandauskas, and Z. Rudzikas, At. Data Nucl. Data Tables **84** (2003) 99.

[27] I.P. Grant, J. Phys. B **7** (1974) 1458.

[28] G. Gaigalas, S. Fritzsche, and I.P. Grant, Comput. Phys. Commun. **139** (2001) 263.

[29] J. Olsen , M. Godefroid, P. Jönsson, P.Å. Malmqvist, and C. Froese Fischer, Phys. Rev. E **52** (1995) 4499.

[30] L. Sturesson, P. Jönsson, and C. Froese Fischer, Comput. Phys. Commun. **177** (2007) 539.

[31] A. Kramida, Yu. Ralchenko, J. Reader, and NIST ASD Team (2013). NIST Atomic Spectra Database (ver. 5.1), [Online]. Available: `http://physics.nist.gov/asd` [2014, January 24]. National Institute of Standards and Technology, Gaithersburg, MD.

[32] G. Gaigalas, Z. Rudzikas and C. F. Fischer,At. Data Nucl. Data Tables **70** (1998) 1.

[33] B. G. Wybourne J. Chem. Phys. **32** (1960) 639.

[34] Z. B. Rudzikas and J. V. Čyplys, Phys. Scr. **T 26** (1989) 21.

[35] G.H. Dieke, Spectra and Energy Levels of Rare Earth Ions in Crystals, Interscience Publishers, New York, 1968, pp. 294-309.

[36] K. W. H. Stevens, Proc. Phys. Soc. A **65** (1952) 209.

[37] B. Bleaney and K. W. H. Stevens Rept. Progr. Phys **16** (1953) 108.

[38] M. T. Hutchings, Solid State Physics **16** (1964) 227.

[39] J.B. Gruber, G.W. Burdick, S. Chandra, and D. K. Sardar, J. Appl. Phys. **108** (2010) 023109.

[40] M. Dammak and De-Long Zhang, Journal of Alloys and Compounds **407** (2006) 8.

[41] N. Magnani, A. Baraldi, E. Buffagni, R. Capelletti, M. Mazzera, S. Brovelli, and A. Lauria, Phys. Status Solidi C **4** (2007) 1209.